

Specification Design and Performances Using Computational Fluid Dynamics for Mini-Remotely Operated Underwater Vehicle

Muhammad Sawal Baital¹, Fakhruddin Mangkusasmito², Mitha Asyita Rahmawaty²

^{1,2,3} Vocational School, University of Diponegoro, Semarang, Indonesia

¹sawalbaital@lecturer.undip.ac.id, ²fakhm17@gmail.com, ³mithaasyitar@lecturer.undip.ac.id

Accepted on 26 April 2022

Approved on 16 June 2022

Abstract— Remotely Operated Underwater Vehicle (ROV) is a submersible robotic system, used to examine various underwater characteristics and controlled by operators from shore. The applications of ROV are widely diverse, especially for exploration and marine industry. This research is to investigate pressure and drag on underwater vehicles using the CFD approach. A low-cost mini ROV with a 300 mm length was used for the research and to determine the hardware and material type required for prototype production by observing pressure and drag from the CFD simulation result. Simulation is solved using CFD software with RANSE method and Shear Stress Transport based $k-\epsilon$ was used as turbulence setting. The result indicated that to pull the mini ROV from the surface to a depth of 50 m requires a thrust of 3,9 kg and the mini ROV receiving the pressure of 7,7 bar.

Index Terms— CFD; Drag; Pressure; ROV

I. INTRODUCTION

Remotely Operated Underwater Vehicle (ROV) is a submersible robotic systems, used to examine various underwater characteristics and controlled by operators from shore[1]. With complex, dangerous and limited areas urgently explored, there is an urgent need for an underwater machine that can replace humans to complete underwater detection. ROV were developed to perform resource exploration tasks in the ocean[2]. The applications of ROV are widely diverse, such as the oil and gas industry, discovery, aquaculture, marine biology, and military purpose [3][4][5][6].

Numerous of ROV designs are assembled around or inside cubic structured frame along with a buoyant on top body. The robotic vehicle utilized umbilical data cable as electrical cable and controlled by operator positioned on surface vessel.

The heavier tools are settled down on lowest possible position to keep the point of center buoyancy is higher than center of gravity, thus adequate stability is obtained. Sufficient stability of ROV meant ROV has capability to withstand against in disturbance for instance moment of rolling and pitch in longitudinal and lateral axis. Steady hydraulic rods suited of lifting

and carrying particular equipment for specific purpose and placed in the fore along with cameras and lights.

Underwater ROVs are generally divided categories based on size, weight, capacity, or performance. Two common design of ROV which widely use are: the ROV Micro-Class with weigh not higher than 3 kg, are used especially in narrow area where a diver might not be capable to enter. And the ROV Mini-Class that weigh about 15 kg are also used as a diver alternative, Inspection-Class are typically rugged ROVs for commercial or industrial use, data acquisition and observation ROVs, Light weight duty category has generally no more than 50 hp on propulsion, While Heavy duty type has less than 220 hp with the ability to capability lift at least two handlers and work at depths up to 3500 m, and Trenching & Burial work class is the largest with more than 200 hp propulsion, with the ability to take a cable, put down sleds and working at depths until 6000 m in several cases[7][8][9][10]. The ROV design and construction is a robust solution to encounter the various require of an ROV to be used in wide implementations, it is compact, handy to use and inexpensive, and allow for confined space exploration. The main form of the body is designed to encounter the particular utilization needs. Commonly, almost ROV attached by torpedo form and an hydrodynamic main body was used at high-speeds[11]. Another type is the torpedo-less form, worked mainly in remote control vehicles (ROVs) that are often worked for shorter period of time purpose or the assessment of other large subsea areas like huge ice floe or water-dams[12]. Toward to emphasize the performance in water resistance, Computational Fluid Dynamics (CFD), drives valuable part in Unmanned vehicle design. Nowadays, CFD approach has been widely applied in underwater vehicle design, as it can simulate the fluid flow field around the bodies and to find out with comprehend the physics of fluid flow phenomenon. CFD captured the flow field such as vortex in very small to major scales which is hard to obtain through field experiments.

CFD methods enable to predict and diagnostic technique for identifying the cause of particular problem in physic phenomena. The latest CFD approaches provide wealth data generated emphasize to

visualize the implication of the result requires considerable skill. Due to this CFD become as an integral part of the design process.

From the economic cost, numerical simulation can deliver result within sufficiently short time span in the design process, thus optimization design can be detailed in addition to addressing this issue during the design process. Numeric simulation is considered low cost analysis hence became early stage to understanding along side with experimental test which can be over cost and intensive time.

In this project, the CFD analysis assists in investigate and demonstrate variable model for the hull body form based on initial prototype [13]. In this research, a design of Mini-ROV is developed especially the principal of body device in each element and electric parts is embedded. Furthermore, the hydrodynamic parameter and analysis was provided based on CFD simulation.

II. METHOD

A. Numerical Modelling

Hydrodynamics reference input was set for the mini-ROV. Therefore simulation of the flow around model is accomplished. The moment coefficient of symmetry flow in both xy plane and xz plane tend to be zero. Physical properties of this simulation conducted at $Re = 8.5 \times 10^5$, $\rho = 1025 \text{ kg/m}^3$, $\nu = 1 \times 10^{-6} \text{ m}^2/\text{s}$ and $U = 1 \text{ m/s}$ or $Fr = 0.6$.

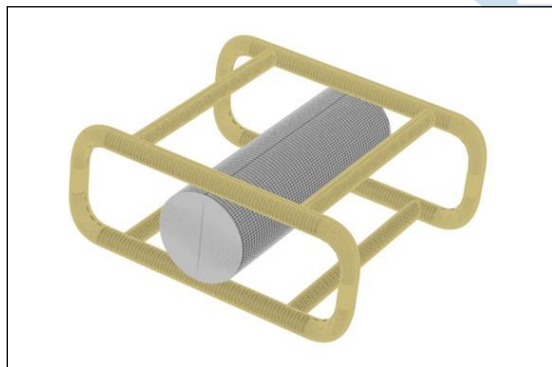


Fig. 1. ROV 3D Model

CFD simulation is used to analyze the total force and pressure difference between horizontal dive, vertical dive, and diagonal dive. The CFD simulation were run on 1:1 scale, 3-Dimension ROV model as shown in Figure 1 and main dimensions of mini-ROV model shown in Table 1.

TABLE I. MAIN DIMENSION

Main Dimension of ROV		
Parts	Unit	Value
Length over all	cm	30
Breadth over all	cm	34
Height over all	cm	14
Main Hull Diameter	cm	10
Support Frame Diameter	cm	2.25
Displacement	kg	3.1

B. Governing Equation RANS

CFD simulation using Reynolds averaged Navier Stokes (RANS) equations implemented in this project, attained by governed general laws for mass, momentum and energy. This method the flow considered as incompressible. The equation of RANS for incompressible flow shown in the following:

$$\frac{\partial \bar{u}_i}{\partial x_i} = 0$$

$$\frac{\partial \bar{u}_i}{\partial t} + \frac{\partial}{\partial x_j} (\bar{u}_i \bar{u}_j + \overline{u'_i u'_j}) = -\frac{1}{\rho} \frac{\partial \bar{p}}{\partial x_i} + \frac{\partial \bar{\tau}_{ij}}{\partial x_j} \quad (1)$$

The derivation of RANS equation from instantaneous of Navier-Stokes equation is the Reynolds decompositions, which refers to separation flow (like velocity u) into mean (time averaged) and fluctuating components (like u') equal to zero.

The subscripts i and j defined the i' and j' components of the cartesian coordinate respectively, \bar{u} and \bar{p} defined the time averaged velocity and pressure respectively, t is the time and ρ is the density of the fluid then $\bar{\tau}_{ij}$ is represent the mean viscous stress tensor.

For the turbulent model adopted k- ω based Shear Stress Transport (SST). Standard k- ω turbulence model is basically combination of k- ω model [14].

The two equation model along with conservation law solved two-transport partial differential equations which acquired turbulence energy diffusion and convection energy. The variables of transport was turbulent kinetic energy (k) indicated turbulent energy and the other was specific turbulent dissipation rate (ω) also known as turbulence scale.

Later k- ω modified with Shear Stress Transport (SST) in order to avoid the k- ω problem of being sensitive to the inlet free-stream turbulence properties [15]. The modified model has capability carried out the transport of the shear stress and satisfied adverse pressure gradient boundary layers and separating flows.

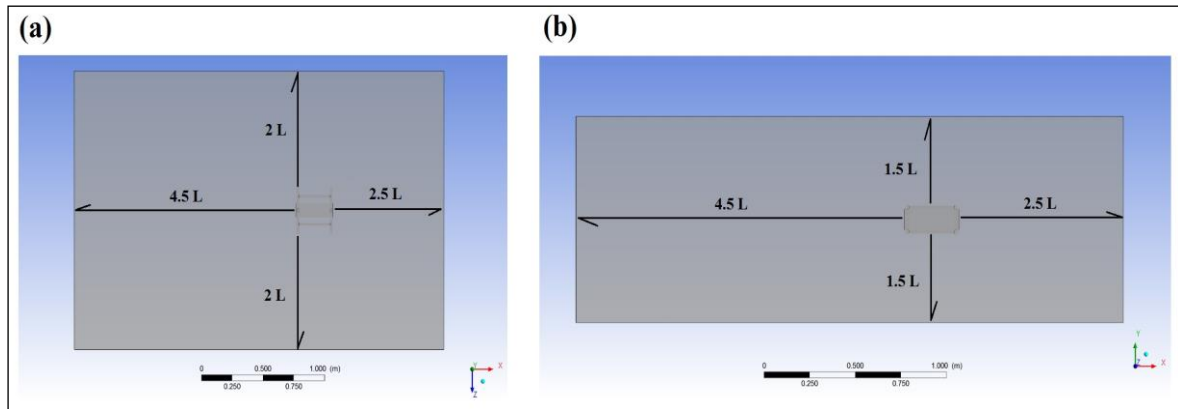


Fig. 2. Computational Domain (a) on XZ plane; (b) on XY plane

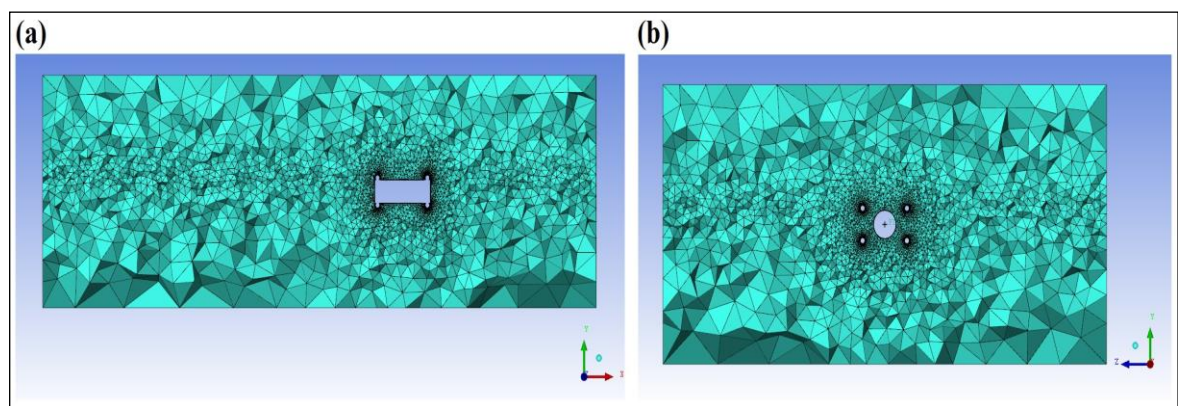


Fig. 3. Unregulated tetrahedral mesh (a) on XY plane; (b) on YZ plane

C. Computational Domain

When conducting CFD numerical simulation, computational domain has significant impact for defining circumstance around the body which engaged with physical condition in fluid dynamics constraint. The space in boundary condition should broad enough to avoid non realistic physic phenomena which lead disrupted the result. The domain spaces where the simulation of numerical solution will be calculated, adequate space let fluid flow surround geometry model did not interfere with boundary domain themselves. The boundary need be discrete in numerous mesh element with structured or unstructured mesh form thus simulation will solved with fluid dynamics equation. The domain came with several shape, in this simulation hexahedron domain was applied. The computational domain for simulation of the ROV model which expressed 2.5L forward the fore of main hull, 4.5L backward the aft of main hull, 2L aside of main hull, 1.5L above upward of the support frame, and 1.5L downward under of the support frame as shown in Figure 2.

D. Boundary and Initial Condition

When attempted CFD analysis, the input of set constraint to the boundary value must be defined and connect the simulation model with its surroundings.

Inlet is defined as flow velocity or known as *velocity inlet*. The turbulent length and turbulent intensity were given for fully developed flow. Outlet identified as *pressure outlet* where the gauge pressure is none or equal to zero. The flow was considered a fully develops, there is no switch turn out in the flow direction and the outlet is designed long distant from the geometrical model disturbances. Wall defined as cube around model. The no-slip condition was determined at whole surface of hexahedron, hence the velocity on surface is zero and there is no stream flow passes through the surface of cube. The final boundary is defined as symmetry was placed at the bottom, top and both sides of the computational domain. The conditions at symmetric boundary are no flow across boundary. The normal velocity and normal gradient of all variable are zero it acted as a mirror that reflects all the flow distribution to the other side. Again any variables have same value and gradients at the same distance from the boundary.

TABLE II. NUMERICAL PROPERTIES

Mesh Properties	
Parameter	Domain Setting
Mesh type	Unregulated tetrahedral mesh
Number of Element	Approximately 1 million

Mesh Properties	
Parameter	Domain Setting
Domain Physics	Continuous fluid (water), SST turbulence model, non buoyant model, reference pressure 1 atm
Boundary Physics	
Parameter	Domain Setting
Inlet	Frictional intensity 0.05, Fluid flow speed Fr 0.3
Outlet	Static pressure 0 Pa
ROV model	No slip condition
Solver Setting	
Parameter	Domain Setting
Turbulence option	First order
Time scale	Physical time scale function 2 sec
Convergence parameter	RMS with residual target 0.00001
Processing parameter	
Parameter	Domain Setting
Run type	Parallel (2 partitions on 4 cores with 16 GB ram)

E. Meshing

CFD is a way of analyzing fluid flows numerically on a computer by a set of algebraic equations. The algebraic equations are obtained by discrete the partial differential equations (PDEs), which may be conservation of mass, momentum, energy etc. The solution is attained at discrete points and hence the computational domains need to be discrete into discrete areas or volume which is the mesh. For this reason, the mesh resolution is of great importance.

The mesh is discrete domain in which the flow problem is to be solved. The flow properties are calculated in every mesh and the density of the cells for instance the mesh resolution is of great importance. Basically, the grid could be either structured or unstructured. In an unstructured mesh such as unregulated tetrahedral, the cells are arranged in an apparently random fashion in contrast to a structured mesh. Mesh generator was carried out to generated mesh for RANS solution.

Unregulated tetrahedral mesh first was generated using Mesh Modeler around the mini-ROV model as shown in Figure 3. Smaller element size of unregulated tetrahedral was used for the ROV model and for the region around the ROV model with refinement is

designate to capture the fluid flow properties and to achieve a finer result. The mesh outside the model, defined as fluid then larger mesh built gradually to reduced time computational aspect.

The mesh number is affected the solution, therefore a convergence process was used in order to achieve mesh independent solutions. If mesh independent is obtained, further refinement of the element does not affect the solution.

F. Numerical Solver Setup

The fluid flow analysis is expressed using CFD based RANS method. Turbulence setting using Shear Stress Transport based $k-\omega$ with turbulence option first order is used to calculate the simulation. Steady state was used for simulation with total elements about 1 million to satisfy mesh independent criteria. This simulation was converged with Residual RMS level 1×10^{-5} was used to investigate. The residual is fundamental measures of an iterative solution convergence, as it directly quantifies the error in the solution of the system of equations. The properties of numerical simulation for fluid flow analysis of ROV model as shown in Table 2.

III. RESULT AND DISCUSSION

A. Mesh Independence

The research was performed using the ROV model with horizontal dive simulation to obtain grid independence solution. Mesh independence used for validating simulation result. The sum of element analyze was used to determine the effect of element number on the calculated total force. To build the mesh, the sum of mesh from domain was sequentially reformed, whilst keeping grow rate parameters and the total element ROV models the same. The results of ROV model at different sum of element for Fr 0.6 from simulations are shown in Table 3. In this case, 6 difference meshes was used to validate mesh independence.

TABLE III. FORCE RESULT AT DIFFERENT TOTAL NUMBER OF ELEMENT

Mesh Independent			
Mesh Number	Number of Element	Total Force	Simulation Running Time
1	cm	30	30 min.
2	cm	34	50 min.
3	cm	14	90 min.
4	cm	10	100 min.
5	cm	2.25	120 min.
6	kg	3.1	200 min.

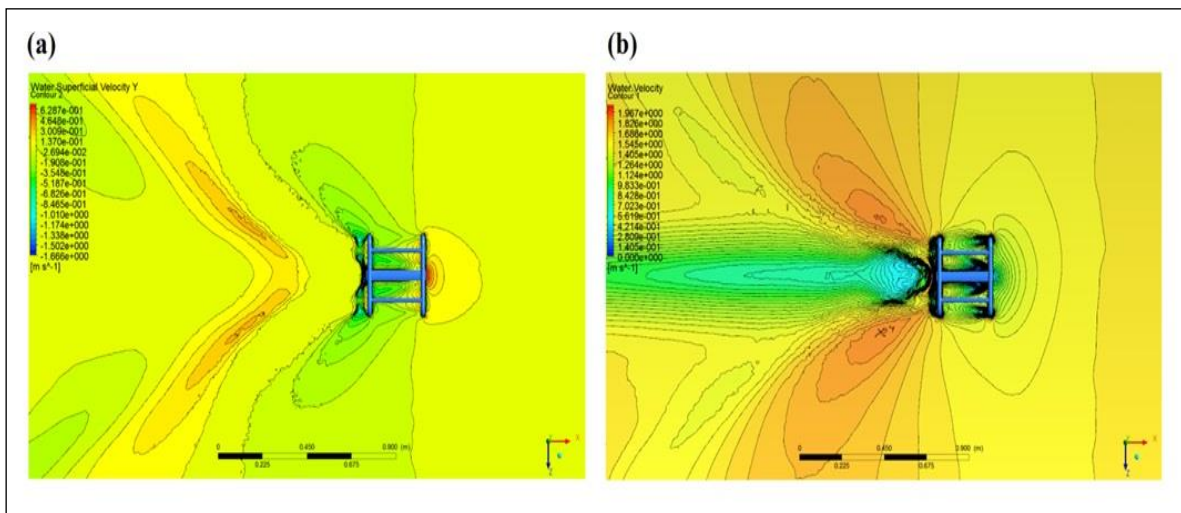


Fig. 4. Flow analysis (a) water superficial velocity contour; (b) velocity contour

The solution converged successfully, with variation of total force as shown in Table 3. In addition, the difference in the total force between Mesh 5 and Mesh 6 are not greater than 2 % [15]. Therefore, the sum of elements on Mesh 5 was chosen and used in all cases of the simulation.

B. The Result of CFD Simulation

Numerical analysis of the ROV model was performed. Computational data was acquired using RANSE code and Turbulence model was selected. The model was run at three particular moves for instance horizontal, diagonal and vertical dive. All cases were run at Fr 0.6 which equals to 2 knots. The model tested in fully submerged simulation which equal 0 to 10 m of depth. The CFD simulation generated physic contour visualization around body mini-ROV model. The movement created phenomena that plot flow pattern in various contour lines. It has color bands that discrete colored regions while the display of a variable on a locator (such as a boundary) shows a finer range of color detail gradually. The contour of water superficial velocity and water velocity are presented in Figure 4(a) and 4(b). The simulation result apparently with diffusion flow of the ROV model respectively. It is mean that the mesh and physical setting was suitable.

Contour of water superficial velocity displayed fluid flow from near to far field that surrounded body mini-ROV model. The contour line appeared caused by fluid mass flow rate through the model. The colors gradation shows difference velocity when fluid flow across the body. The stream assumed the only flow mass rate through passed the model and whereby

estimated rapidly the fluid flowing through the medium. In figure 4(a) water superficial velocity has various speed ranges. Superficial velocity performed volumetric flow rate per sectional area. Both in portside and starboard mini-ROV model has interchangeable flow pattern which has similar velocity and considered low. On contrary in front of body has high velocity at middle spot region. It caused by stagnation point on fore body mini-ROV. On rear body has larger flow pattern with few variant fluid flow velocity.

Figure 4(b) illustrate water velocity contour, this velocity contour displayed actual fluid flow velocity. It meant the velocity of fluid flow travelled significant distance per time. Even though has same unit with superficial velocity (m/s), water velocity has detailed in small region. The figure shown on rear body mini-ROV has significant contour, fluid velocity fell dropped compared to other areas. Rear body has transom formed, where body has not streamlined which lead the fluid particle did not fully transmitted far away behind body hence suddenly suffered small turbulence[16].

In CFD simulation, the value of total drag and total pressure caused by ROV movement was obtained directly, the result shown in table 4, 5 and 6. It shows the value at each step Froude number, with unit Newton in total drag and Pascal in total pressure respectively. This value became major lead reference in determining motor thrust. Since the mini-ROV mostly operated in horizontal dive, hence the value at service speed (Fr 0.6) was discussed. Total drag and total pressure 11.863 N and 94.704 Pa. It is meant that motor installed at ROV must be has a thrust of 4 kg, to run ROV at operational speed.

TABLE IV. TOTAL DRAG AND PRESSURE OF ROV MODEL (HORIZONTAL DIVE)

Total Drag Horizontal Dive						
Fr	Speed in Knot	Total drag		Total pressure		
0.30	1.00	2.963 N	0.302 kgf	23.345 Pa	6.663 kg/m2	0.667 kg
0.45	1.50	6.891 N	0.702 kgf	63.364 Pa	10.744 kg/m2	1.809 kg

Total Drag Horizontal Dive						
<i>Fr</i>	<i>Speed in Knot</i>	<i>Total drag</i>		<i>Total pressure</i>		
0.52	1.75	9.971 N	1.016 kgf	81.125 Pa	12.556 kg/m ²	2.316 kg
0.60	2.00	11.863 N	1.209 kgf	94.704 Pa	13.940 kg/m ²	2.704 kg
0.75	2.50	13.252 N	1.351 kgf	153.424 Pa	19.927 kg/m ²	4.381 kg
0.82	2.75	14.034 N	1.431 kgf	168.258 Pa	21.440 kg/m ²	4.804 kg

TABLE V. TOTAL DRAG AND PRESSURE OF ROV MODEL (DIAGONAL DIVE)

Total Drag Diagonal Dive						
<i>Fr</i>	<i>Speed in Knot</i>	<i>Total drag</i>		<i>Total pressure</i>		
0.30	1.00	5.024 N	0.512 kgf	40.856 Pa	8.449 kg/m ²	1.166 kg
0.45	1.50	10.036 N	1.023 kgf	79.765 Pa	12.416 kg/m ²	2.277 kg
0.52	1.75	14.014 N	1.429 kgf	106.585 Pa	15.151 kg/m ²	3.043 kg
0.60	2.00	17.536 N	1.788 kgf	124.748 Pa	17.003 kg/m ²	3.562 kg
0.75	2.50	20.022 N	2.041 kgf	168.224 Pa	21.437 kg/m ²	4.803 kg
0.82	2.75	22.032 N	2.246 kgf	185.752 Pa	23.224 kg/m ²	5.304 kg

TABLE VI. TOTAL DRAG AND PRESSURE OF ROV MODEL (VERTICAL DIVE)

Total Drag Vertical Dive						
<i>Fr</i>	<i>Speed in Knot</i>	<i>Total drag</i>		<i>Total pressure</i>		
0.30	1.00	5.962 N	0.608 kgf	14.945 Pa	5.807 kg/m ²	0.427 kg
0.45	1.50	11.264 N	1.148 kgf	40.065 Pa	8.368 kg/m ²	1.144 kg
0.52	1.75	15.037 N	1.533 kgf	56.675 Pa	10.062 kg/m ²	1.618 kg
0.60	2.00	18.785 N	1.915 kgf	71.377 Pa	11.561 kg/m ²	2.038 kg
0.75	2.50	21.412 N	2.183 kgf	106.554 Pa	15.148 kg/m ²	3.042 kg
0.82	2.75	22.658 N	2.310 kgf	117.145 Pa	16.228 kg/m ²	3.345 kg

Figure 5(a) shows of value total drag in Newton unit toward rate of Froude number (Fr). From this graph total drag of three movement dive was increased at every step Froude number. The vertical and diagonal dive has similar coincide trend which sharply increased from Fr 0.3 to Fr 0.6 and then slowly growth until Fr 0.8. Contrast with horizontal dive which considered slightly increased and then steadily increase.

From the trends show the vertical dive has highest value and the horizontal dive has lowest value of total drag at the service speed or Fr 0.6. The total drag of horizontal is less than 12 N and vertical dive has almost 19 N. Both of dives motion has significant difference up to 32%. Diagonal dive has slightly lower than vertical dive. This different caused by ROV motion against fluid flow that commonly called angle of attack.

In other hand Figure 5(b) shown graph of the total pressure value in Pascal (Pa) unit toward rate of Froude number (Fr). The trends of three movement model has similar pattern. Each of motion has significant rose at each step Froude number. This graph displays diagonal dive has highest quantity and the vertical dive has lowest quantity at service speed model.

Total pressure of diagonal dive has around 15 Pa and vertical dive has about 70 Pa, which means vertical dive took only a half. In addition value of total pressure

horizontal dive slightly higher than the vertical dive with approximately 95 Pa. The huge gap of diagonal and vertical dive happened caused by ROV body form travelled against fluid flow.

The detail visualization about affected of total pressure around body ROV has shown in Figure 6(a), 6(b), and 6(c). This CFD simulation captured physic phenomena around body due to fluid flow respectively. When mini ROV travelled through fluid flow, the pressure force acting on each element of body surface summed over entire body to produce total pressure. The pressure arose from viscous of fluid flow.

The figure 6(a) illustrated total pressure of body mini-ROV which simulation capture the pressure mostly affected at side of body. The figure 6(b) demonstrated total pressure of body mini-ROV when moved diagonally. It shown that diagonal dive has affected pressure on almost surface area and has biggest total pressure value among the movement. When body moved diagonally both side and bottom affected pressure that push perpendicular integrally. The last figure 6(c) described vertical dive. Same as horizontal dive, it has one side affected major pressure area, which is bottom region of mini ROV. This pressure acted normally to the body.

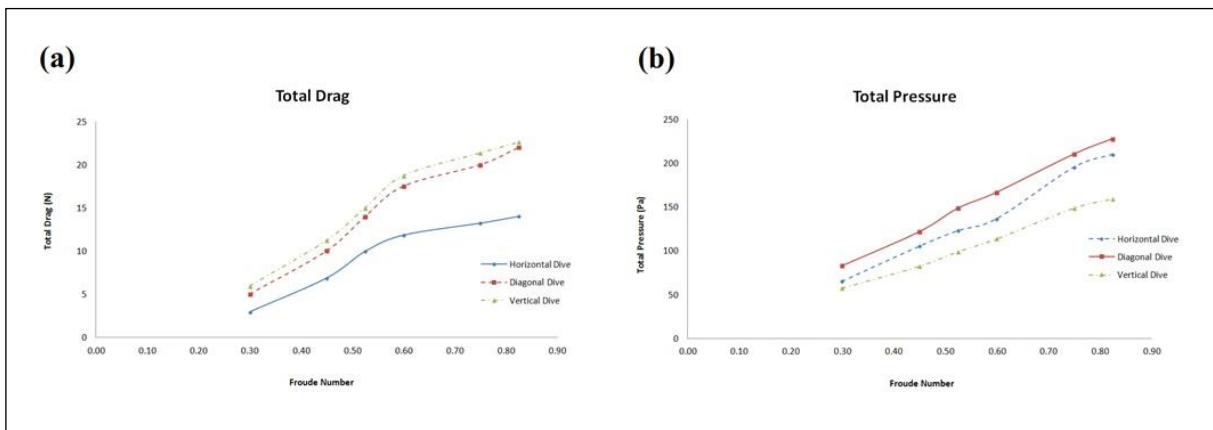
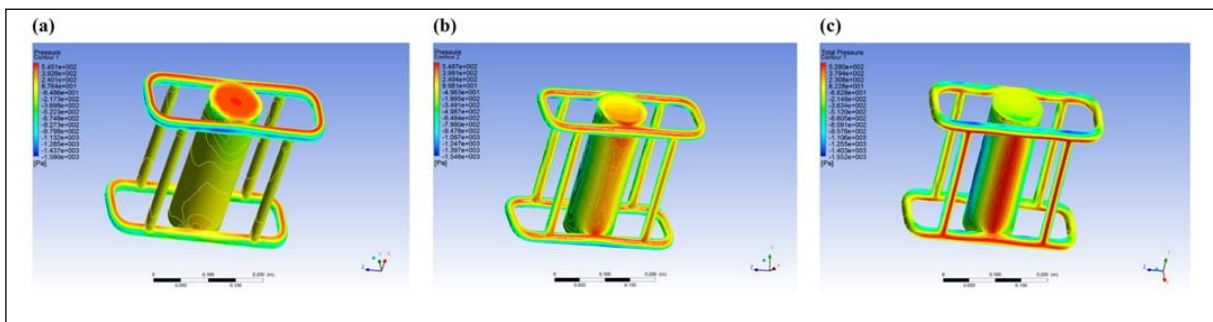


Fig. 5. Simulation Result (a) Total Drag; (b) Total Pressure 1



Total Pressure of ROV body form (a) Horizontal Dive; (b) Diagonal Dive; (c) Vertical Dive

IV. MATERIAL PRODUCTION AND CONTROLLER

A. Material Production

According to CFD analysis result regarding pressure value, the material of ROV main body was selected. Polyvinyl Chloride (PVC) with category rigid PVC known as Unplasticized PVC (PVC-U) was chosen to accommodate the requirement value of pressure. UPVC materials are used in the broad transportation of drinking water, water sewage and soil, underground drainage and industrial applications and eco-friendly which meant allow to disposable. UPVC has high hardness mechanical properties of tensile strength up to 51 MPa, thus body ROV allowed to free dive below the sea conducted with CFD result.

B. Controller Hardware

In Addition, Mini ROV was propelled by thruster with BLDC type of brushless motor fitted 4 kg of thrust power to overcome due to impact of the resistance where acted around mini ROV body up to 3.562 kg at Fr 0.6. Thus Mini ROV was allowed to travel under the sea. The velocity and axial rotation of BLDC motor controlled by 12 Volt BLDC motor driver circuit then operated by Arduino UNO R3.

V. CONCLUSION

ROV has major role for environmental research and surveying underwater purpose for evidence, especially

the micro-ROV with light body geometry can reach through narrow and dangerous area. It provides a cost-effective alternative to fully utilize research grants and funding. The investigation of mini ROV using simulation CFD based RANSE software was successfully determined. Hydrodynamic parametric has been accomplished particularly in total force and total pressure. CFD simulation provides comprehend visualization of fluid flow around body thus performance of ROV can be examined.

When performing numerical analysis, it is important to ensure that the numerical errors are as small as possible. Except from the error associated with the fact that the solution is attained at discrete points in the domain, there are three important sources of error. First the governing equations need to be able to describe the fluid flow in a satisfactory way, this lead to the second source of error which is the algebraic equations and lastly the physical model used in the simulation (e.g. turbulence models).

The total force is used to determined amount of motor thrust with around weigh 4 kg. Then total pressure is employed the load pressure can be hold up about 8 bar when ROV operated and diving depth into underwater. The mini ROV succeed fulfill of design and performance requirement. Further research for mini ROV still developed to adjust in many research fields.

ACKNOWLEDGMENT

The authors are thankful to Vocational School Faculty, University of Diponegoro for partially funding the study.

REFERENCES

- [1] A. M. Tahir and J. Iqbal, "UNDERWATER ROBOTIC VEHICLES: LATEST DEVELOPMENT TRENDS AND POTENTIAL CHALLENGES," *Sci.Int.(Lahore)*, 2014.
- [2] M. Nancekievill et al., "Detection of simulated fukushima daichii fuel debris using a remotely operated vehicle at the naraha test facility," *Sensors (Switzerland)*, 2019.
- [3] V. Raoult et al., "Remotely operated vehicles as alternatives to snorkellers for video-based marine research," *J. Exp. Mar. Bio. Ecol.*, vol. 522, 2020.
- [4] Rahimuddin, H. Hasan, H. A. Rivai, Y. Iskandar, and P. Claudio, "Design of Omni Directional Remotely Operated Vehicle (ROV)," 2018.
- [5] R. Jones and J. Drabble, "U.K.'s submarine rescue efforts," *Sea Technol.*, 1993.
- [6] L. Bezanson, S. Reed, E. M. Martin, J. Vasquez, and C. Barbalata, "Coupled control of a lightweight ROV and manipulator arm for intervention tasks," 2017.
- [7] A. Costanza, G. D'Anna, A. D'Alessandro, and G. Vitale, "Micro-ROV instrumental customization and canister design under pressure," 2017.
- [8] J. H. Tarneckii and W. F. Patterson, "A mini ROV-based method for recovering marine instruments at depth," *PLoS One*, 2020.
- [9] R. Capocci, G. Dooly, E. Omerdić, J. Coleman, T. Newe, and D. Toal, "Inspection-class remotely operated vehicles-a review," *Journal of Marine Science and Engineering*, vol. 5, no. 1. 2017.
- [10] T. H. Samosir, K. W. A. Masengi, P. N. I. Kalangi, M. Iwata, and I. F. Mandagi, "Aplikasi remotely operated vehicle (ROV) dalam penelitian kelautan dan perikanan di sekitar perairan Sulawesi Utara dan Biak Papua," *J. ILMU DAN Teknol. Perikan. TANGKAP*, 2012.
- [11] M. Chyba, T. Haberkorn, R. N. Smith, and S. K. Choi, "Autonomous Underwater Vehicles: Development and Implementation of Time and Energy Efficient Trajectories," *Sh. Technol. Res.*, 2008.
- [12] A. Amory and E. Maehle, "Modelling and CFD Simulation of a Micro Autonomous Underwater Vehicle SEMBIO," 2019.
- [13] C. S. Chin, W. P. Lin, and J. Y. Lin, "Experimental validation of open-frame ROV model for virtual reality simulation and control," *J. Mar. Sci. Technol.*, 2018.
- [14] D. C. Wilcox, *Turbulence modeling for CFD*. 1993.
- [15] J. D. Anderson and J. D. Anderson Jr, *Computational Fluid Dynamics The Basics with Applications*. 1995.
- [16] F. D. Kurniawati and I. K. A. Pria Utama, "An Investigation into the Use of Ducktail at Transom Stern to Reduce Total Ship Resistance," *IPTEK J. Proc. Ser.*, 2017.

